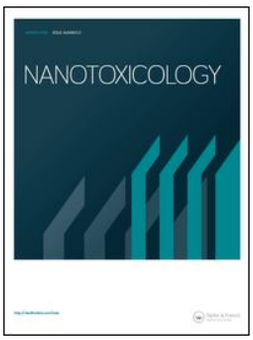

Nanotoxicology

ISSN: 1743-5390 (Print) 1743-5404 (Online) Journal homepage: https://www.tandfonline.com/loi/inan20

Acute systemic exposure to silver-based nanoparticles induces hepatotoxicity and NLRP3-dependent inflammation

Khalil B. Ramadi, Yassir A. Mohamed, Ashraf Al-Sbiei, Saeeda Almarzooqi, Ghada Bashir, Aisha Al Dhanhani, Dhanya Sarawathiamma, Shahnaz Qadri, Javed Yasin, Abderrahim Nemmar, Maria J. Fernandez-Cabezudo, Yousef Haik & Basel K. Al-Ramadi

To cite this article: Khalil B. Ramadi, Yassir A. Mohamed, Ashraf Al-Sbiei, Saeeda Almarzooqi, Ghada Bashir, Aisha Al Dhanhani, Dhanya Sarawathiamma, Shahnaz Qadri, Javed Yasin, Abderrahim Nemmar, Maria J. Fernandez-Cabezudo, Yousef Haik & Basel K. Al-Ramadi (2016) Acute systemic exposure to silver-based nanoparticles induces hepatotoxicity and NLRP3-dependent inflammation, Nanotoxicology, 10:8, 1061-1074, DOI: 10.3109/17435390.2016.1163743

To link to this article: https://doi.org/10.3109/17435390.2016.1163743

http://tandfonline.com/inan
ISSN: 1743-5390 (print), 1743-5404 (electronic)

Nanotoxicology

Nanotoxicology, 2016; 10(8): 1061–1074
 DOI: 10.3109/17435390.2016.1163743

Taylor & Francis
Taylor & Francis Group

ORIGINAL ARTICLE

Acute systemic exposure to silver-based nanoparticles induces hepatotoxicity and NLRP3-dependent inflammation

Khalil B. Ramadi[1]*, Yassir A. Mohamed[1], Ashraf Al-Sbiei[1], Saeeda Almarzooqi[2], Ghada Bashir[1], Aisha Al Dhanhani[1], Dhanya Sarawathiamma[1], Shahnaz Qadri[3], Javed Yasin[4], Abderrahim Nemmar[5], Maria J. Fernandez-Cabezudo[6], Yousef Haik[3]**, and Basel K. Al-Ramadi[1]

[1]*Department of Medical Microbiology & Immunology, and* [2]*Department of Pathology, United Arab Emirates University, Al Ain, United Arab Emirates,* [3]*Department of Mechanical Engineering, College of Engineering, United Arab Emirates University, Al Ain, United Arab Emirates,* [4]*Department of Internal Medicine and* [5]*Department of Physiology, United Arab Emirates University, Al Ain, United Arab Emirates, and* [6]*Department of Biochemistry, College of Medicine and Health Sciences, United Arab Emirates University, Al Ain, United Arab Emirates*

Abstract

Nanoparticles (NPs) are increasingly being commercialized for use in biomedicine. NP toxicity following acute or chronic exposure has been described, but mechanistic insight into this process remains incomplete. Recent evidence from *in vitro* studies suggested a role for NLRP3 in NP cytotoxicity. In this study, we investigated the effect of systemic administration of composite inorganic NP, consisting of Ag:Cu:B (dose range 1–20 mg/kg), on the early acute (4–24 h post-exposure) and late phase response (96 h post-exposure) in normal and NLRP3-deficient mice. Our findings indicate that systemic exposure ($\geq$2 mg/kg) was associated with acute liver injury due to preferential accumulation of NP in this organ and resulted in elevated AST, ALT and LDH levels. Moreover, within 24 h of NP administration, there was a dose-dependent increase in intraperitoneal neutrophil recruitment and upregulation in gene expression of several proinflammatory mediators, including TNF-α, IL-1β and S100A9. Histological analysis of liver tissue revealed evidence of dose-dependent hepatocyte necrosis, increase in sinusoidal Kupffer cells, lobular granulomas and foci of abscess formation which were most pronounced at 24 h following NP administration. NP deposition in the liver led to a significant upregulation in gene expression of S100A9, an endogenous danger signal recognition molecule of phagocytes, IL-1β and IL-6. The extent of proinflammatory cytokine activation and hepatotoxicity was significantly attenuated in mice deficient in the NLRP3 inflammasome, demonstrating the critical role of this innate immune system recognition receptor in the response to NP.

Keywords

Acute nanotoxicity; hepatotoxicity; IL-1β; NLRP3; S100A9; silver nanoparticles

History

Received 7 May 2015
Revised 19 January 2016
Accepted 2 March 2016
Published online 11 April 2016

Introduction

Engineered nanoparticles (NPs) are increasingly being utilized in a host of consumer products and in the development of novel drug delivery systems, vaccines and diagnostics. Current estimates suggest that silver nanoparticles (AgNPs), due largely to their well-characterized anti-microbial activity (Kim et al., 2007), are the most widely used NP in consumer products industry, including textiles, cosmetics, electronics, medical and personal hygiene supplies and pharmaceuticals (Dos Santos et al., 2014). With the increasing likelihood of human exposure to NP through inhalation, ingestion, direct skin contact or injection, our understanding of the cellular and molecular basis for NP-associated potential toxicities has lagged behind (Nemmar et al., 2014; Valsami-Jones & Lynch, 2015). Although metallic elements are considered biologically inert, the potential for NPs to have a toxic effect stems from their unique physical characteristics. While their small size grants them remarkable physicochemical properties, being the same order of magnitude in size as subcellular organelles makes them more likely to interfere with intracellular pathways and mechanisms (Nel et al., 2006).

Studies investigating potential NP toxicities using *in vitro* cell line culture systems demonstrated concentration-, and particle size-, dependent cytotoxic and genotoxic effects on a variety of mammalian cell types following exposure to NP. The addition of TiO_2, crystalline silica or AgNP to dendritic cells, human lung epithelial cells or blood monocytes, respectively, resulted in the induction of an inflammatory response, as manifested by activation of caspase-1 and increased secretion of IL-1β (Peeters et al., 2013; Winter et al., 2011; Yang et al., 2012). Silica NPs are able to penetrate into the nucleus of human epithelial cells, disrupting nuclear functioning and inhibiting replication, transcription and cell proliferation (Chen & von Mikecz, 2005). Similar *in vitro* studies have shown that cells co-cultured with NPs show elevated reactive oxygen species (ROS) levels, and displayed

*Present Address: Harvard-MIT Health Sciences and Technology Division, Massachusetts Institute of Technology, Cambridge, MA, USA. **Present Address: Department of Mechanical Engineering, Qatar University, Doha, Qatar.

Correspondence: Dr. Basel K. al-Ramadi, Department of Medical Microbiology & Immunology, College of Medicine and Health Sciences, United Arab Emirates University, P.O. Box 17666, Al Ain, United Arab Emirates. E-mail: ramadi.b@uaeu.ac.ae

subsequent apoptotic and necrotic behavior (Carlson et al., 2008; Foldbjerg et al., 2009).

Exposure of human blood monocytes and primary bronchial epithelial cells to NP induces the release of inflammatory mediators, predominantly through NOD-like receptor containing pyrin domain 3 (NLRP3) inflammasome-dependent mechanism (Jung et al., 2014; Peeters et al., 2013; Yang et al., 2012). Carbon black NPs were also found to induce pyroptosis, an inflammasome-dependent mode of cell death, in cultured human alveolar macrophages (Reisetter et al., 2011). Moreover, TiO_2 and SiO_2, but not ZnO, NPs were shown to induce pulmonary inflammation through the activation of the NLRP3 inflammasome (Yazdi et al., 2010). Collectively, these findings suggest that NLRP3 inflammasome is involved in the response to some types of NP (Sun et al., 2013).

A few studies have also been published that highlighted AgNP-related toxicities in experimental animals following oral (Cha et al., 2008; Ebabe Elle et al., 2013), inhaled (Smulders et al., 2014; Sung et al., 2009) or systemic (Li et al., 2014; Sarhan & Hussein, 2014) exposure to NP. However, the potential role of NLRP3 inflammasome in NP-mediated toxicities *in vivo* has not been examined previously. As such, our understanding of the mechanisms underlying these toxicities remains incomplete. Moreover, it is not known whether NP-induced cytotoxicity is solely a reflection of their remarkable ability to penetrate through cellular membranes, causing damage to various organelles, or is mediated through a physiological process of recognition by cellular sensors leading to an inflammatory reaction. Apparently conflicting data showing lack of any toxicity following oral gavage of AgNP was also recently reported (Bergin et al., 2016), highlighting the need for further studies to refine our understanding of this important public health issue.

Here, we assessed the consequences of systemic delivery of composite Ag:Cu:B nanoclays in wild-type and NLRP3-deficient mice. We provide evidence that acute systemic exposure to NP leads to the induction of strong acute inflammatory response, recruitment of neutrophilic granulocytes into the site of administration and preferential accumulation of NP in the liver leading to hepatotoxicity. These effects are abated in mice deficient in the NLRP3 inflammasome, implicating this protein as the main cellular sensor for NP.

Materials and methods

Mouse strains

BALB/c and C57BL/6 mice were purchased from Harlan Olac (Bicester, Oxfordshire, UK). NLRP3-deficient mice on C57BL/6 background (Sutterwala et al., 2006) were generously provided by Dr. Richard Flavell (Yale University School of Medicine, New Haven, CT). Mice were bred in our animal facility and maintained in filter-topped isolator cages with a controlled light and dark cycle of 12 h each at 24–26 °C. For the present studies, male mice were used in experiments at 8–12 weeks of age. They were maintained on standard laboratory animal diet with food and water *ad libitum*. All studies involving animals were conducted in accordance with and after approval of the Animal Research Ethics Committee of the Faculty of Medicine and Health Sciences, United Arab Emirates University.

Synthesis and physical characterization of NPs

Copper (II) sulfate 99.0% (Cat #C1297), silver nitrate 99.0% (Cat#6506), sodium hydroxide 97.0 (Cat#21160), boric acid 99.5% (Cat#B6768) were obtained from Sigma (St. Louis, MO). NPs were synthesized by chemical co-precipitation method in which 0.1 M of metal salts of copper sulfate and silver chloride and boric acid in a ratio of 70:20:10 (Ag:Cu:B) were heated up to 90 °C in a triple neck flask under vigorous stirring by a Teflon double blade with the aid of a homogenizer under argon atmosphere. An 8 M solution of NaOH was added drop wise until the formation of black precipitate. The precipitate was heated for 20 min until turned to grayish black color. The precipitate was washed three times in deionized water and then centrifuged for 10 min at 4000 rpm. The pellet was sonicated for 1 h in an ice bath to reduce the temperature rise during sonication. The sample was filtered through Whatman filter paper and dried under vacuum overnight. Dried NPs were stored at room temperature in a closed vessel. To minimize agglomeration, for each experiment NPs were weighed from dried stock, suspended in PBS/0.01% Tween-80, sonicated and used immediately for injection. Old stock in suspension was discarded to avoid aggregation of the particles due to the formation of copper oxide. Hitachi cold field emission scanning electron microscope (CFe-SEM S4800) with Oxford EDS (energy-dispersive X-ray spectrometer), Malvern Zetasizer and inductively coupled plasma-optical emission spectrometry (ICP-OES) were used to characterize the synthesized particles. Size measurements on the SEM images were performed by Quartz 8 imaging software. Elemental identification was provided by EDS Oxford spectroscopy using INCA software for acquiring the X-ray spectrum from point of interest. Only two particles were selected to obtain the X-ray spectrum in order to minimize the interference from surrounding material. Point analysis was used in which two NPs were highlighted for elemental analysis at 130,000× magnification, accelerating voltage 20 kV, process time = 5, live-time of 250 and real time of 288.7. Malvern Zetasizer and ICP-OES were used to characterize the synthesized particles. One milliliters of 10 mg/ml of NP was digested in 5% nitric acid with final concentration of 10 ppm in a volumetric flask that was covered by aluminum foil to protect it from light and was kept for 2 h at room temperature. Standard addition method was used to detect the concentration of silver, copper and boron. Standard curves were generated by standard addition method in which samples were spiked with 1, 5 and 10 ppm from multi-element standard solution containing silver, copper and boron in a final volume with 5% nitric acid. Calibration test was passed for all three elements with detection limit of 50 ppb for each.

In vivo toxicity studies

These studies were carried out as previously described (Fernandez-Cabezudo et al., 2013). Briefly, mice (3–5 mice per experimental group) were injected i.p. with saline or NP (dose range 1–20 mg/kg). At the indicated time points, blood was collected by venipuncture of the inferior vena cava into EDTA-containing tubes and cell counts of the total WBC, RBC and platelets were determined by an ABX VET ABC hematology analyzer with a mouse card (ABX Diagnostics, Montpellier, France). Chemistry analysis of the blood including hemoglobin, creatinine, BUN, ALT, AST and LDH was performed by standard laboratory methods using a commercially available kit produced by Roche (Basel, Switzerland) in blood chemistry analyzer (Roche COBAS, Switzerland). For all *in vivo* studies, mice were monitored on a daily basis for signs of morbidity (rapid weight loss, dehydration, slow movement). Moribund mice were routinely euthanized by CO_2 asphyxiation.

Detection of metal (Ag, Cu and B) ions in organ homogenates

Metal ion concentration in organ homogenates was determined by ICP-OES (Fernandez-Cabezudo et al., 2007). Animal organs (liver, kidney, heart, lung and brain) were aseptically removed at

the indicated time points following NP inoculation, weighed and a portion cut out and processed in 1 ml ice-cold saline using a tissue homogenizer (Ultra-terrax T25; Janke & Kunkle, Staufenim Breisgau, Germany), as previously described (al-Ramadi et al., 2006). The homogenate was mixed with 6 ml of spectroscopy grade 5% nitric acid (Sigma Aldrich), vortexed for 2 min and then incubated for 24 h in ice cold conditions. The acid digested-samples were made up to 15 ml with deionized water and filtered to remove any debris. The filtered samples were used for ICP-OES analysis.

Histology and immunohistochemistry of liver tissue

Liver tissue was processed for histological analysis following a previously published procedure (al-Ramadi et al., 2009). Briefly, livers were resected and fixed in 10% formalin, dehydrated through graded ethanol, and embedded in paraffin for permanent sections. Paraffin embedded tissues were sectioned serially at 25 µm intervals of 5 µm thickness using a rotary microtome (Shandon AS 325, Pittsburgh, PA). Sections were deparaffinized, rehydrated and stained with haematoxylin and eosin (H&E), then dehydrated in ascending concentrations of ethanol, cleared in xylene and mounted in DPX (Panreac, Navarra, Spain). Staining for liver macrophages was done using F4/80-specific mAb (Cat.# T-2006, BMA Biomedicals, Augst, Switzerland). Images were captured using Olympus BX53 microscope equipped with digital camera DP26 (Tokyo, Japan).

Antibodies and flow cytometry

Analysis of peritoneal exudate cells (PECs) was carried out using a six-color FACS analysis, following a standard procedure (Issac et al., 2013; Kaimala et al., 2014). Cells were stained with a combination of directly conjugated mAbs, washed and analyzed using FACSCanto II (BD Biosciences, Mountain View, CA). The antibodies used were CD11b-APC-Cy7, CD3-FITC and CD19-PE (BD Biosciences, CA), F4/80-PE-Cy7 and Ly6G-APC (eBioscience, San Diego, CA). Non-viable cells staining positive with 7AAD dye (eBioscience) were excluded from the analysis. Data collected on 50,000 cells were analyzed using FACSDiva software (BD Biosciences).

Quantitative RT-PCR analysis

Analysis of gene expression in PECs was carried out as previously described (Kaimala et al., 2014). For this study, qRT-PCR was also carried out on liver RNA extracted from a portion of the organ from each animal. Following RNA extraction and purification, cDNA was synthesized using Taqman reverse transcription reagents (Applied Biosystems, Foster City, CA) according to manufacturer's protocol. Premade TaqMan primers and probes (Applied Biosystems) were used to study the expression of the inflammatory markers IL-1β, IFN-γ, IL-6 and S100A9. Primers for the specific detection of TNF-α cDNA were custom made by Metabion International AG (Steinkirchen, Germany). The TNF-α primer sequences are F: 5′-CCT CCC TCT CAT CAG TTC TAT-3′ and R: 5′-CTA GTT GGT TGT CTT TGA GAT CC-3′. The TNF-α probe sequence is: 5′-6-Fam-ACA AGC CTG TAG CCC ACG TCG TAG-BHQ-1-3. Transcript levels of target genes were normalized according to the Δ*C*q method to respective mRNA levels of the housekeeping gene HPRT. Unless otherwise indicated, the expression of the target gene is reported as the level of expression relative to HPRT.

Statistical analysis

Statistical significance between multiple experimental groups was analyzed using the unpaired, two-tailed Student's *t*-test, using the statistical program of GraphPad Prism version 6 software (San Diego, CA). Differences between experimental groups were considered significant when p values were <0.05.

Results

Properties of NPs

The synthesized NPs used in this study varied in size and were rectangular in shape. Figure 1(A) shows the size distribution of the particles. The size ranged from 20 to 260 nm with average particle size around 100 nm. As shown in Figure 1(B), the EDS results gave a silver to copper ratio in the order of 70.23:17.36. Boron was difficult to be identified by EDS because of its low atomic number. To confirm the composition of the NP, ICP-OES 700 was used. The concentrations were found be 69:20:14 for Ag, Cu and B, respectively. Malvern Zetasizer (Nano Z) laser Doppler micro-electrophoresis was used to measure the zeta potential. Fresh dried particles were suspended in deionized water (concentration 10 mg/ml) and sonicated to ensure homogeneous solution before the zeta potential measurements. The zeta potential provided the charge −30 mV 229 indicating low solubility and moderate colloidal suspension (Figure 1C).

In vivo toxicity and association with NP deposition in organs

Healthy adult BALB/c mice were tested in an acute exposure model following i.p. injection of NP suspension at doses ranging from 1 mg/kg to 20 mg/kg concentration. No mortality was recorded in any experimental group over the observation period of 96 h. Animals receiving the highest dose of NP appeared sluggish 24 h after injection, but they recovered well and showed no further signs of morbidity up to 96 h post-exposure. Following NP administration at 1 mg/kg or 2 mg/kg dose, mice were sacrificed at either 4 h or 24 h time point and their blood was collected for hematology and clinical chemistry analysis. The results of the hematology analysis, shown in Figure 2, indicate no gross abnormalities except for a small but significant decrease in white blood cell (WBC) and platelet count (PLT) in mice injected with 2 mg/kg NP dose, especially at 24 h post-inoculation (Figure 2A and B, respectively). Moreover, no alterations in red blood cell count or hemoglobin concentration were observed (Figure 2C and D, respectively). In contrast, clinical chemistry analysis revealed significant elevation in ALT, AST and LDH in mice receiving high NP dose (Figure 3A–C) but, no changes in kidney markers, including BUN (Figure 3D) and creatinine (data not shown) were observed. To determine whether these changes are directly related to NP deposition in organs, we determined NP concentrations in different organ homogenates 4 h post-injection of NP (Figure 3E). The data indicate a distinct and preferential accumulation of silver ions in the liver. These findings correlate with the results showing elevated ALT and AST levels, while blood hematology and kidney function metabolite levels remaining largely within normal range. We thus hypothesize that acute exposure to high concentrations of NP can result in acute liver damage and toxicity, leading to elevated liver enzyme levels.

Accumulation of metallic ions in various organs in WT and NLRP3-deficient mice

The NLRP3 inflammasome has previously been implicated in the recognition of some types of NP (Simard et al., 2015; Yazdi et al., 2010). To investigate the potential role of NLRP3 in the observed nanotoxicity, we first determined the biodistribution of NP in wild-type C57BL/6 (WT) and NLRP3-deficient ($NLRP3^{-/-}$) mice 4 h following i.p. inoculation with 2 mg/kg NP. The concentrations of Ag, Cu and B were determined in liver,

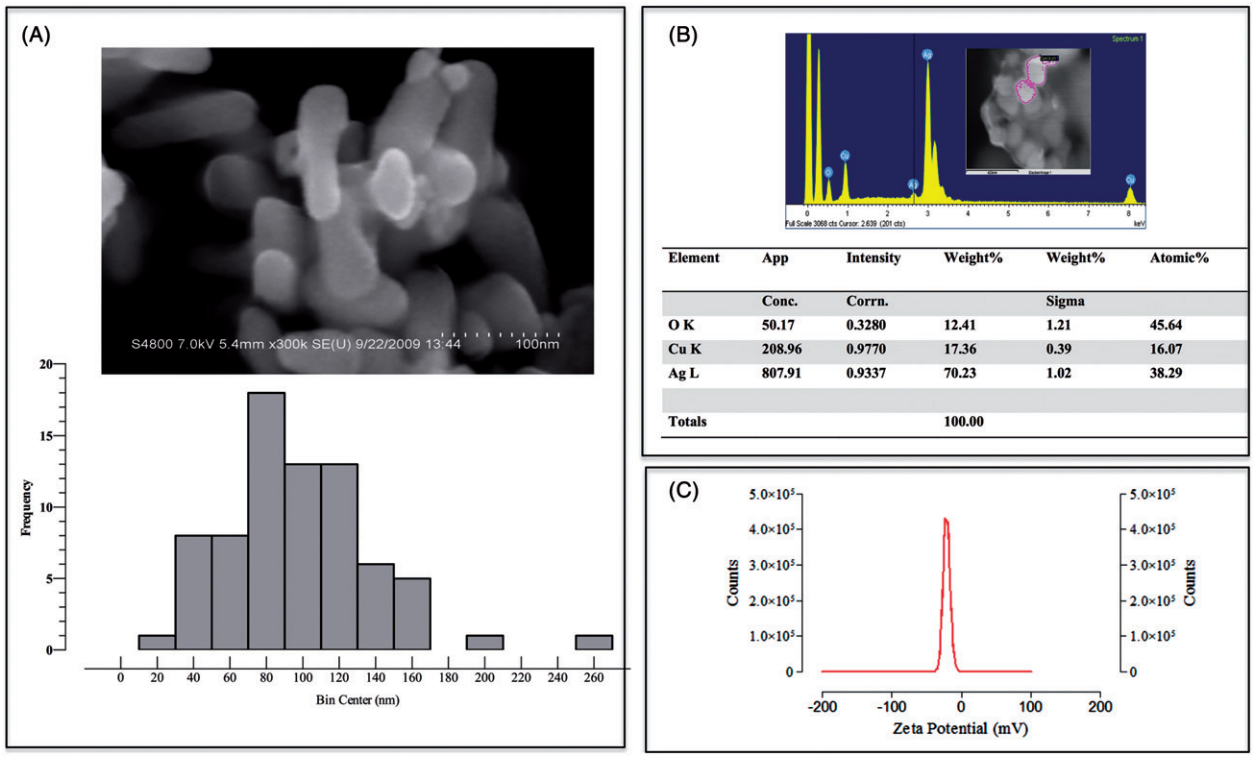

Figure 1. Physical characteristics of NP. (A) Particle size distribution using size analysis with insert of SEM monograph obtained using FE_SEM S-4800 Hitachi shows rectangular shape nanoparticles. The average size ranges between 80 and 140 nm. The size measurements were performed using Quartz-8 imaging software. (B) Oxford's energy dispersive X-ray spectroscopy (EDS) elemental analysis. The EDS peaks show presence of silver, copper and oxygen. Copper is oxidized to CuO and Cu_2O, which justifies the presence of oxygen. (C) Zeta potential measured by M3-PALS (Phase Analysis Light Scattering) technique. The zeta potential for the NP was −30 mV.

kidney, lung, heart and brain tissue (Figure 4). The highest levels of Ag were detected in the livers of both mouse strains following NP injection, representing >5-fold increase over control mice (panel *A*). AgNPs were also detected above normal levels in the lungs and hearts. In contrast, the levels of Cu and B detected in all organs were not different from control mice (panels *B* and *C*). The data suggest that i.p. administration of AgNP leads to their accumulation primarily in the livers of both WT and NLRP3$^{-/-}$ mice.

Reduced NP-induced liver toxicity in NLRP3-deficient mice

Next we investigated the potential role of NLRP3 in NP-induced toxicity using a range of doses (1–20 mg/kg) and determined the resulting effects at an early (24 h) and late (96 h) time points. WT and NLRP3$^{-/-}$ mice were inoculated with NP and tested for plasma levels of liver enzymes AST and ALT and for LDH as a general tissue toxicity marker (Figure 5A–E). The data demonstrate that NP injection led to significant elevations in AST, ALT and LDH levels in WT mice, which were prominent at 24 h (Figure 5A, C, E). At the same time point, similarly treated NLRP3$^{-/-}$ mice exhibited no significant increases in AST or ALT enzymes (Figure 5A, C), but a marginal increase in LDH at the highest NP dose was observed (Figure 5E). By 96 h, WT animals have mostly normalized all enzyme levels, with only AST showing slightly elevated level compared to control (Figure 5B, D, F). Interestingly, there was a delayed response in NLRP3$^{-/-}$ mice to NP administration, as evidenced by the modest, but significant, increase in ALT and AST levels observed at 96 h in mice treated with 2 or 20 mg/kg doses (Figure 5D). Elevated LDH levels were also observed in these animals following exposure to the highest NP dose (Figure 5F). Thus, in WT mice, elevated AST, ALT and LDH levels represent part of a rapid response to an acute systemic NP exposure and appear to be transient in nature as these levels normalize by 96 h post-treatment. In contrast, NLRP3$^{-/-}$ mice exhibit a significantly diminished response early after NP injection but a delayed elevation in ALT, AST and LDH levels is evident by 96 h.

Exposure to NP induces an influx of inflammatory myeloid cells into the peritoneal cavity

The changes in PECs were assessed following NP inoculation by immunophenotyping by multi-color flowcytometry using a combination of CD11b, F4/80, Ly6G, CD19 and CD3-specific mAbs. This analysis was done at early (24 h) and late (96 h) time points following systemic exposure to a dose of 1, 2, or 20 mg/kg. Representative results from this analysis (24 h; 2 mg/kg NP dose) are shown in Figure 6A–H, and the data summary from both time points is given in Figure 6, graphs *I–J*. Overall, the findings demonstrate that administration of NP into WT or NLRP3$^{-/-}$ mice induces a significant influx of CD11b$^+$ myeloid cells into the peritoneal cavity (Figure 6A–D), which was dependent on the dose of NP used (Figure 6I–J). At 24 h post-exposure, although infiltration of both macrophages and neutrophils was evident, the cellular influx was primarily due to neutrophils (CD11b$^+$ Ly6G$^+$ cells) in both mouse strains (panels *E–H* and *I–J*). In WT control mice, the percentage of neutrophils was 3.0 ± 1.3, which was increased to 21.4 ± 2.9, 29.6 ± 4.4 and 45.6 ± 2.3 following injection 1, 2 or 20 mg/kg NP, respectively (Figure 6J). Similar cellular alterations were observed in NLRP3$^{-/-}$ mice, where the corresponding values were 2.4 ± 0.6 (control group) and 21.2 ± 1.1, 24.6 ± 4.7 and 40.7 ± 4.4 for NP-injected groups, respectively (Figure 6*J*). The cellular constituents of the peritoneal cavity undergo a dramatic shift towards predominant macrophages (CD11b$^+$ F4/80$^+$ cells) at 96 h post-inoculation, where they represent around 60% of the total PECs (Figure 6J).

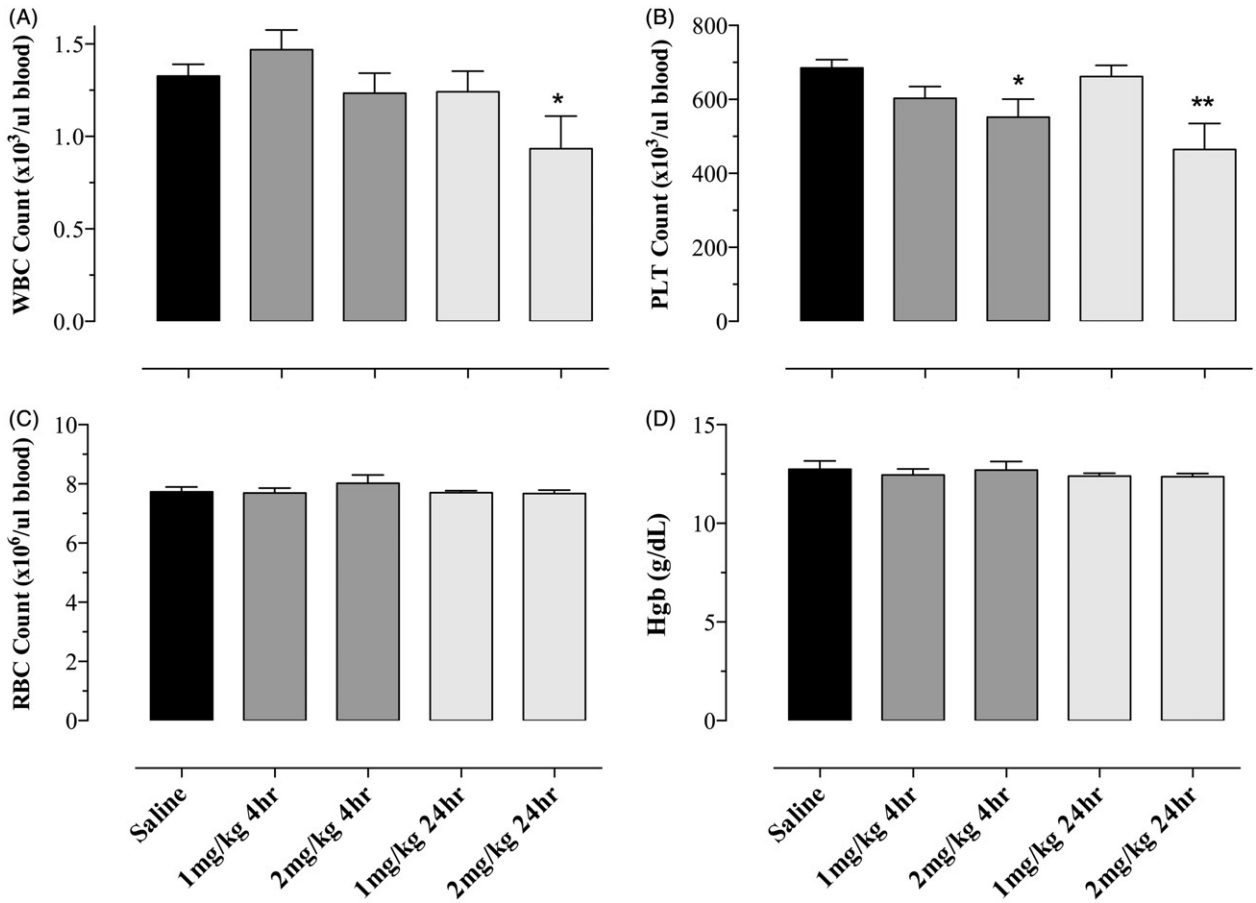

Figure 2. Hematology parameters following systemic administration of NP. BALB/c mice (five per group) were injected i.p. with saline or composite metallic NP at doses of 1 or 2 mg/kg of body weight. Blood was collected after 4 and 24 h and analyzed for (A) white blood cell (WBC), (B) platelet (PLT) and (C) red blood cell (RBC) counts. (D) Hemoglobin (Hgb) concentration was also determined. The results are representative of at least five independent experiments. Asterisks denote statistically significant differences between indicated experimental group and the saline control group (*$p \leq 0.05$, **$p \leq 0.01$).

Interestingly, very similar cellular alterations were observed in WT as well as NLRP3$^{-/-}$ mice. Thus, administration of NP induces an early influx of neutrophils (by 24 h) followed by macrophages at 96 h. These waves of cellular infiltrations in response to NP inoculation appear to be independent of NLRP3 inflammasome.

Acute inflammation in response to NP inoculation

The consequence of NP injection on peritoneal lavage cells was examined by quantitative analysis of gene expression using qPCR. Inflammation is associated with upregulation of many genes; however, for this study, we selected three well-characterized markers of inflammation, S100A9, IL-1β and TNF-α for further analysis. Following i.p. injection of a single dose of NP (dose range: 1–20 mg/kg), peritoneal cells were harvested at 24 h or 96 h and processed for qPCR analysis. As shown in Figure 7, the expression of all three genes was strongly upregulated in WT mice at 24 h post-NP inoculation (Figure 7A, C, E). In comparison with saline-treated mice, the fold-increase in S100A9 gene expression was 16.7, 22.6 and 97.6 using 1, 2 or 20 mg/kg NP dose (Figure 7A). Similarly, dose-dependent induction of IL-1β was evident, with fold increases of 11.9, 7.2 and 73.7 being observed following injection of 1, 2, or 20 mg/kg NP (Figure 7B). Significant induction of TNF-α was only seen at the highest dose of NP, with no detectable expression in saline-control mice (Figure 7C). Interestingly, inoculation of NP into age and sex-matched mice lacking the NLRP3 inflammasome resulted in significantly lower levels of expression of the S100A9 and IL-1β genes but equivalent TNF-α expression (Figure 7A, C and E). In terms of fold change compared to control, the corresponding fold increases for S100A9 in NLRP3$^{-/-}$ mice were 3.2, 4.6 and 34.9 (Figure 7A). For IL-1β cytokine, despite lower relative expression in NLRP3$^{-/-}$ compared to WT mice, calculation of fold change compared to NLRP3$^{-/-}$ control revealed equivalent levels of gene induction (fold increases of 5.4, 4.9 and 106.3, respectively) in both mouse strains (Figure 7C). Analysis of gene expression changes at 96 h post-NP inoculation revealed decreased levels of S100A9 and IL-1β in NLRP3$^{-/-}$ mice but equivalent levels of TNF-α in both mouse strains (Figure 7B, D, F). We have also assessed changes in IL-6 and IFN-γ gene expression in PECs following NP administration but the findings revealed no significant induction in either mouse strain with all NP doses used (Supplementary Figure). Taken together, these data show that i.p. administration of NP leads to a dose and time-dependent upregulation in gene expression of inflammatory mediators. This response is differentially attenuated in NLRP3$^{-/-}$ mice.

The observed changes in gene expression are most likely due to direct entry of NPs into myeloid cells, causing cellular stress. To investigate the potential contribution of LPS contamination of NP suspension to the observed activation of proinflammatory genes, NPs were suspended in saline buffer and then spun down and removed before the buffer was injected i.p. into mice. qPCR gene expression analysis of mice inoculated with NP-washed

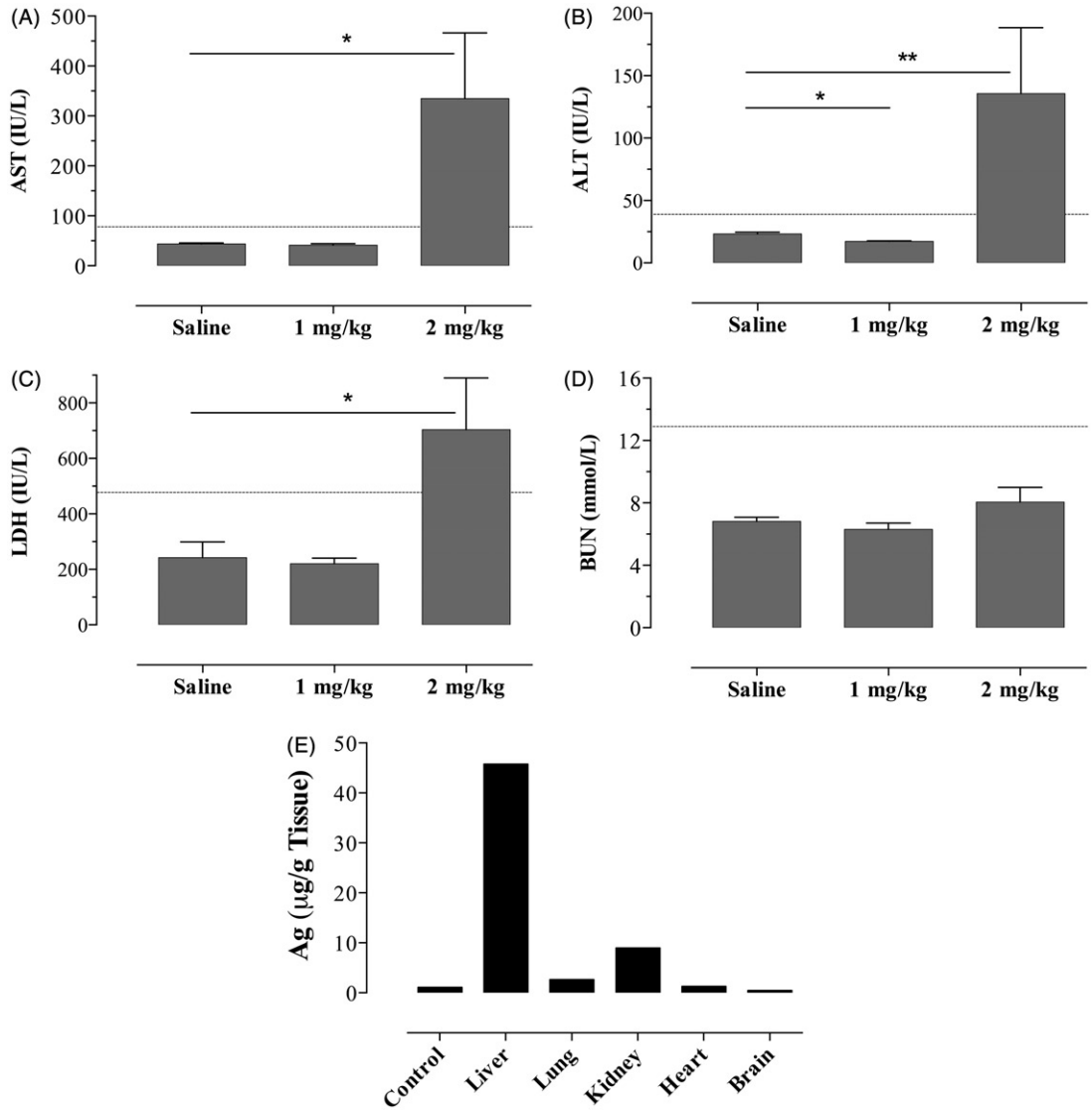

Figure 3. Injected NPs accumulate in the liver and induce an increase in liver enzymes. BALB/c mice ($n = 5$) were injected i.p. with saline or NP (at 1 or 2 mg/kg body weight). Blood plasma was collected after 4 h and analyzed for (A) AST, (B) ALT, (C) LDH and (D) BUN levels. The dotted line in each graph depicts the normal upper limit. The results are representative of at least five independent experiments. Asterisks denote statistically significant differences between indicated experimental group and the saline control group ($*p \leq 0.05$, $**p \leq 0.01$). (E) Mice were injected i.p. with saline or NP (2 mg/kg). Four hours later, mice were sacrificed and liver, lung, kidney, heart and brain were collected. Organs from five mice per group were pooled and processed for analysis of Ag ionic content by inductively coupled plasma-optical emission spectrometry (ICP-OES). Liver tissue from saline-injected mice was used as background control. The results are representative of three independent experiments.

saline showed no evidence of gene induction, ruling out the possibility that any LPS contamination of NP suspensions being responsible for the observed gene expression profile in NP-injected animals (data not shown).

Deposition of NP in liver tissue induces NLRP3-dependent inflammation

Gene expression analysis was carried out on liver tissue obtained from control and NP-exposed WT and NLRP3-deficient mice. This analysis was undertaken using representative liver portions obtained at 24 h and 96 h following i.p. administration of NP. The findings demonstrate dose-dependent activation of S100A9, IL-1β and IL-6 genes (Figure 8A, C, E) as early as 24 h post-exposure in WT mice. Significant upregulation of S100A9 was evident even at low NP doses, with 5.9, 6.5 and 49.9-fold increase being observed using 1, 2 or 20 mg/kg NP doses (Figure 8A). After 4 days of NP inoculation, S100A9 gene expression remained significantly elevated compared to the control group. Interestingly, however, the level of expression was significantly reduced compared to the early time point, with the fold changes being only 2.8, 2.7 and 9.2-fold at three NP doses, respectively (Figure 8B). In contrast, expression of S100A9 gene was minimally induced in NLRP3$^{-/-}$ mice (4.0- and 8.2-fold increase) 24 h following administration of 2 or 20 mg/kg NP doses, while at 96 h no significant upregulation was seen (Figure 8A and B). Significant increase in IL-1β and IL-6 gene expression was observed in WT, but not in NLRP3$^{-/-}$, mice receiving the highest NP dose at 24 h post-injection (Figure 8C and E). There was no evidence for any significant increase in IL-1β or IL-6 gene expression at the 96 h time point in either strain of mice (Figure 8D and F). We also assessed the expression of IFN-γ in liver tissue following NP administration but no significant induction in either mouse strain, at all NP doses, was observed (Supplementary Figure). These findings demonstrate that NP-triggered upregulation of S100A9, IL-1β and IL-6 proinflammatory genes in the liver is dose- and time-dependent and requires the NLRP3 inflammasome.

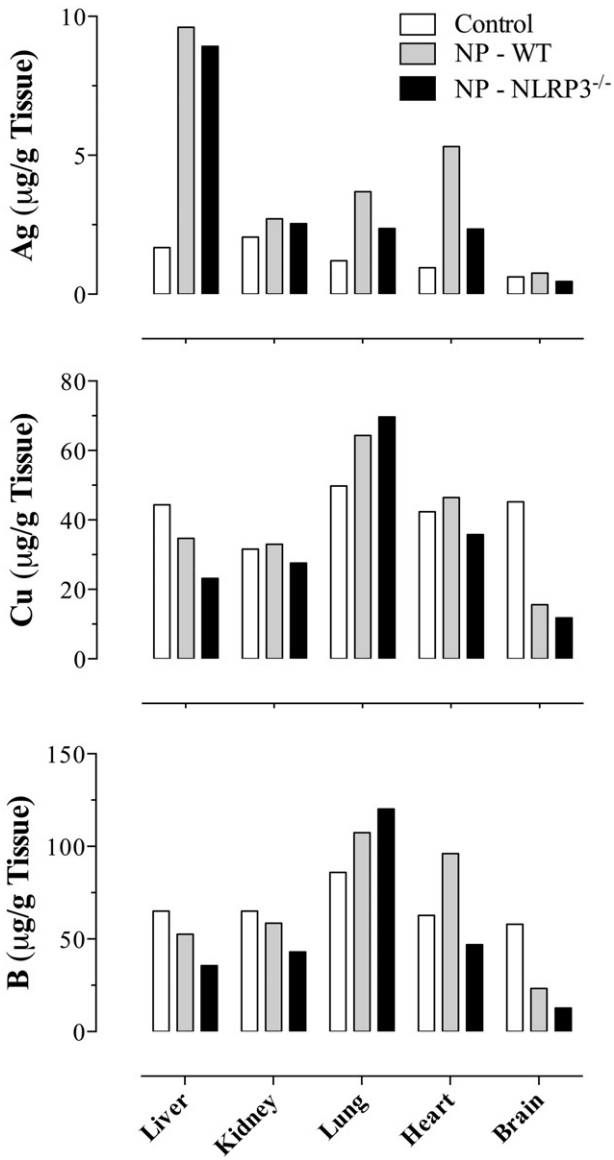

Figure 4. Comparative tissue biodistribution of NP in C57BL/6 (WT) and NLRP3$^{-/-}$ mice. Four hours following exposure to NP (2 mg/kg), indicated organs were aseptically removed, individually weighed, pooled from five mice per experimental group, and analyzed by ICP-OES. Control tissues were obtained from saline-treated WT and NALP3$^{-/-}$ mice, both of which providing similar background levels for each element. The results are representative of two independent experiments.

Histological and immunohistochemical analysis of liver tissue

The consequence of NP administration on liver tissue was examined by histological analysis of liver sections of WT and NLRP3$^{-/-}$ mice obtained 24 h or 96 h after injection of NP at different doses (1–20 mg/kg body weight). H&E staining of liver sections of saline-treated WT or NLRP3$^{-/-}$ mice (both at 24 h and 96 h) showed a preserved hepatic architecture with no evidence of significant portal or lobular inflammation and no overt hepatocyte necrosis or apoptosis. There were rare areas with occasional lobular aggregates of few histiocytes (Figure 9; panels *A*, *D*, *G*, *J*). Assessment of WT liver tissue treated with NP (20 mg/kg) at 24 h revealed the presence of large multiple foci of abscess formation, characterized by a central necrotic zone with a mixed inflammatory infiltrate of neutrophils, lymphocytes and histiocytes and a peripheral rim of necrotic hepatocytes (Figure 9B). Zones of necrotic hepatocytes, characterized by loss of nuclei, dense eosinophilic homogenous cytoplasm and preservation of cellular outline, a pattern akin to a coagulative-type necrosis, were also observed. Moreover, an interesting finding was the presence of a mixed inflammatory cell infiltrate at the capsule or outer surface of the liver samples which was associated with necrosis of the adjacent hepatocytes (Figure 9C). Immunohistochemical evaluation using F4-80 mAb highlighted the sinusoidal Kupffer cells and focal lobular collection of histiocytes (data not shown). Assessment of liver tissue sections of animals treated with 1 mg/kg NP revealed a similar pattern to that of normal, saline-treated, controls (data not shown). Animals exposed to 2 mg/kg NP showed overall mild changes including focal areas with lobular inflammatory infiltrate, but necrosis was rarely observed (data not shown).

In contrast, liver histology findings in NLRP3$^{-/-}$ mice at 24 h revealed the presence of similar foci of coagulative type necrosis but without an overt inflammatory response surrounding them or any abscess formation (Figure 9E). This reaction appears to be a milder form or an earlier phase or a delayed slowed response in comparison to that observed in WT mice (Figure 9B). In addition, the capsule demonstrates a mixed inflammatory infiltrate with necrosis of some adjacent hepatocytes (Figure 9F) but this appears to be less severe in comparison to the inflammatory infiltrate seen in WT mice (Figure 9C).

Liver analysis of WT animals, which were inoculated with NP (20 mg/kg) 96 h previously, demonstrated focal areas of hepatocyte death similar to coagulative type necrosis characterized by loss of nuclear details, dense eosinophilic homogenous cytoplasm and an associated inflammatory infiltrate (Figure 9H). In addition, features indicative of hepatocyte injury were noted and included hepatocyte disarray and formation of pseudoacini. The foci were noticeably smaller in size and number than those noted in the corresponding group at 24 h post-exposure. Moreover, the capsule of the liver was unremarkable and lacked any inflammatory infiltrate (Figure 9I). Examination of 96 h-liver sections of NP-injected NLRP3$^{-/-}$ mice demonstrated similar but less severe findings. Foci of hepatocyte necrosis with associated inflammatory infiltrate were now observed and consisting only of few or single hepatocyte necrosis within the inflammatory focus (Figure 9K). The liver capsule appeared intact but was associated with minimal inflammatory infiltrate consisting of few eosinophils and lymphocytes (Figure 9L).

Collectively, the observed liver changes in WT animals are consistent with the induction of an acute inflammatory response and hepatotoxicity as a result of the administration of NP that was maximal at 24 h. These changes were dependent on the dose of NP used (data not shown) and appeared to be less severe by 96 h after exposure. In contrast, in the absence of the NLRP3 inflammasome, the acute liver response to NP seemed to be less severe and with delayed kinetics compared to WT mice.

Discussion

Nanomaterials are being increasingly utilized in biomedical applications including drug delivery, diagnostics and targeting of therapeutic drugs. Such drug administration inherently necessitates a systemic delivery of NPs. We have developed novel nanoalloys of Ag–Cu–B metals for potential use as antimicrobial compounds against typically problematic human bacterial pathogens such as multidrug-resistant *S. aureus*. The NP alloy consists of Ag, Cu and B (at 70:20:10 ratio, respectively) with Ag and Cu metals contributing to its anti-bacterial properties and B providing the stability for a prolonged release of Ag and Cu ions from the complex. The aim of the present study was to investigate the potential immunotoxicity associated with the use of these nanoalloys *in vivo* and characterize the underlying mechanisms

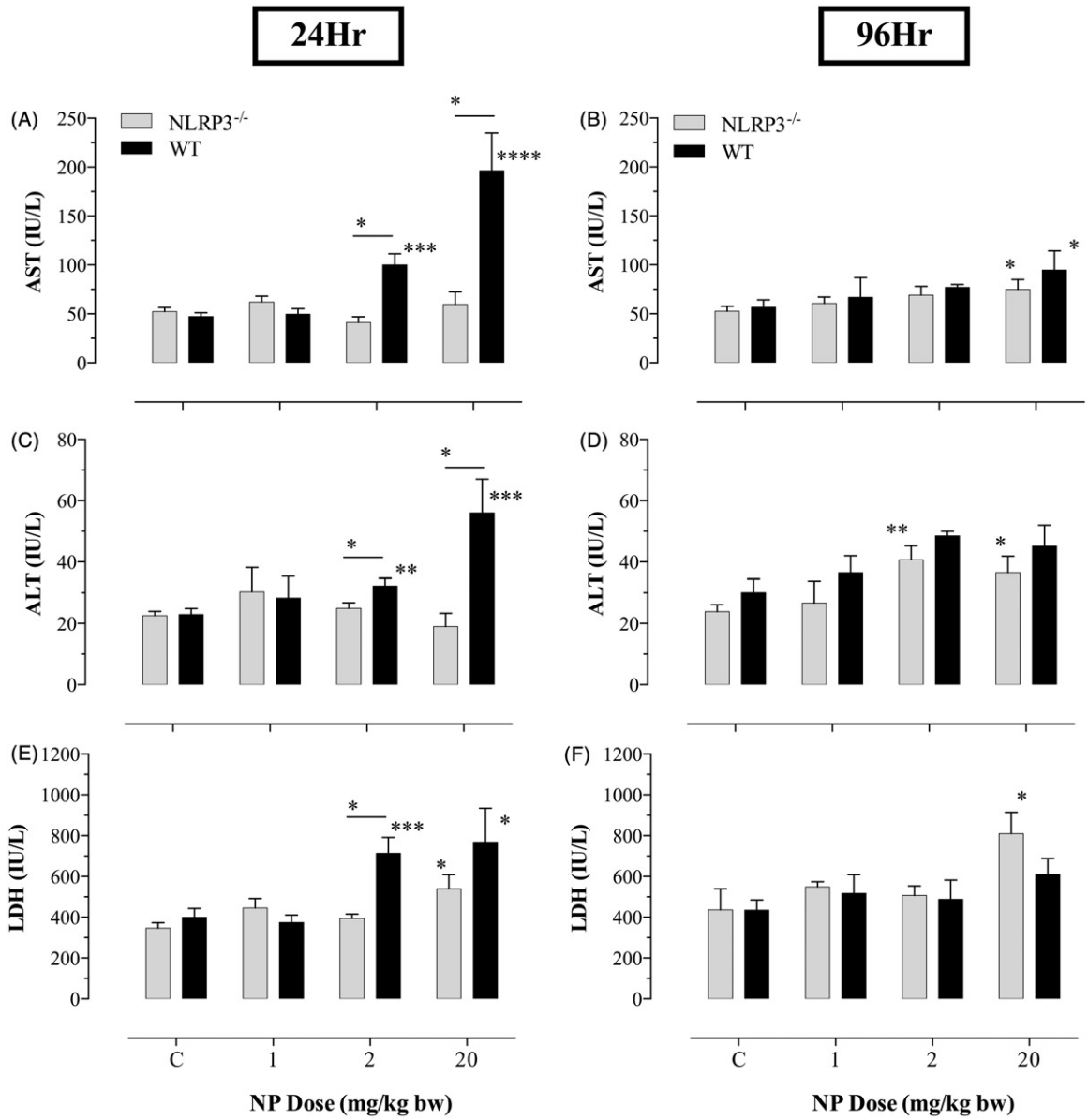

Figure 5. Reduced response to NP in NALP3$^{-/-}$ mice. C57BL/6 (WT) and NLRP3$^{-/-}$ mice were injected i.p. with saline (C = control) or with 1, 2 or 20 mg/kg dose of NP ($n = 5$ per group). At 24 h or 96 h after injection, plasma was collected and analyzed for AST (*A–B*), ALT (*C–D*) and LDH (*E–F*) levels. The results are representative of three independent experiments. Asterisks denote significant differences between the indicated experimental groups (*$p \leq 0.05$, **$p \leq 0.01$, ***$p \leq 0.001$, ****$p \leq 0.0001$). Additionally, when present, asterisks above each bar denote significant differences in comparison to the control, saline-injected, group.

involved. Our findings demonstrate that intraperitoneal inoculation of metallic nanoalloys leads to an acute inflammatory cytokine response, with the NP depositing primarily in the liver and resulting in elevated levels of serum liver enzymes within 4 h of administration. The extent of elevated liver enzymes in the serum was dependent on the dose of NP and began to normalize over 96 h post-exposure. Moreover, NP-induced inflammatory cytokine response was evident in the liver and peritoneal cavity and was maximal at 24 h following NP injection. Based on our findings, the minimum dose of Ag nanoalloys that results in observable liver toxicity was 2 mg/kg body weight. Using NLRP3$^{-/-}$ mice we demonstrate, for the first time, that AgNP-triggered acute inflammation in the liver is significantly reduced in the absence of the NLRP3 inflammasome, highlighting an important role for NLRP3 in the response to Ag-based nanoalloys.

Concern over the toxicity of fine particles originally stemmed from the advent of fuel burning. From coal to diesel, all combustion processes release micro-sized particles into the atmosphere. In large concentrations, these particles can cause lung inflammation and subsequent systemic toxicity (Borm, 2002). However, similar toxicity problems have been reported with NP. In a rat chronic oral exposure model, administration of AgNP over a 90-day period resulted in their preferential accumulation in the liver resulting in organ toxicity (Kim et al., 2010). Based on these findings, a dose of 125 mg/kg was identified as showing the lowest observable adverse effect level in rats following oral exposure to AgNP. In another study, exposure to high dose AgNP in diet over 81 days resulted in raised oxidative stress and liver inflammatory markers, including ALT, IL-6 and TNF-α (Ebabe Elle et al., 2013). Exposure through inhalation, intractracheal instillation or oropharyngeal aspiration of AgNP resulted in their deposition in lungs and liver and induced a predominantly Th2-type inflammatory response and tissue damage in the lungs of affected animals (Park et al., 2011; Smulders et al., 2014; Sung et al., 2009). Moreover, exposure to AgNP led to the induction of proinflammatory cytokines and

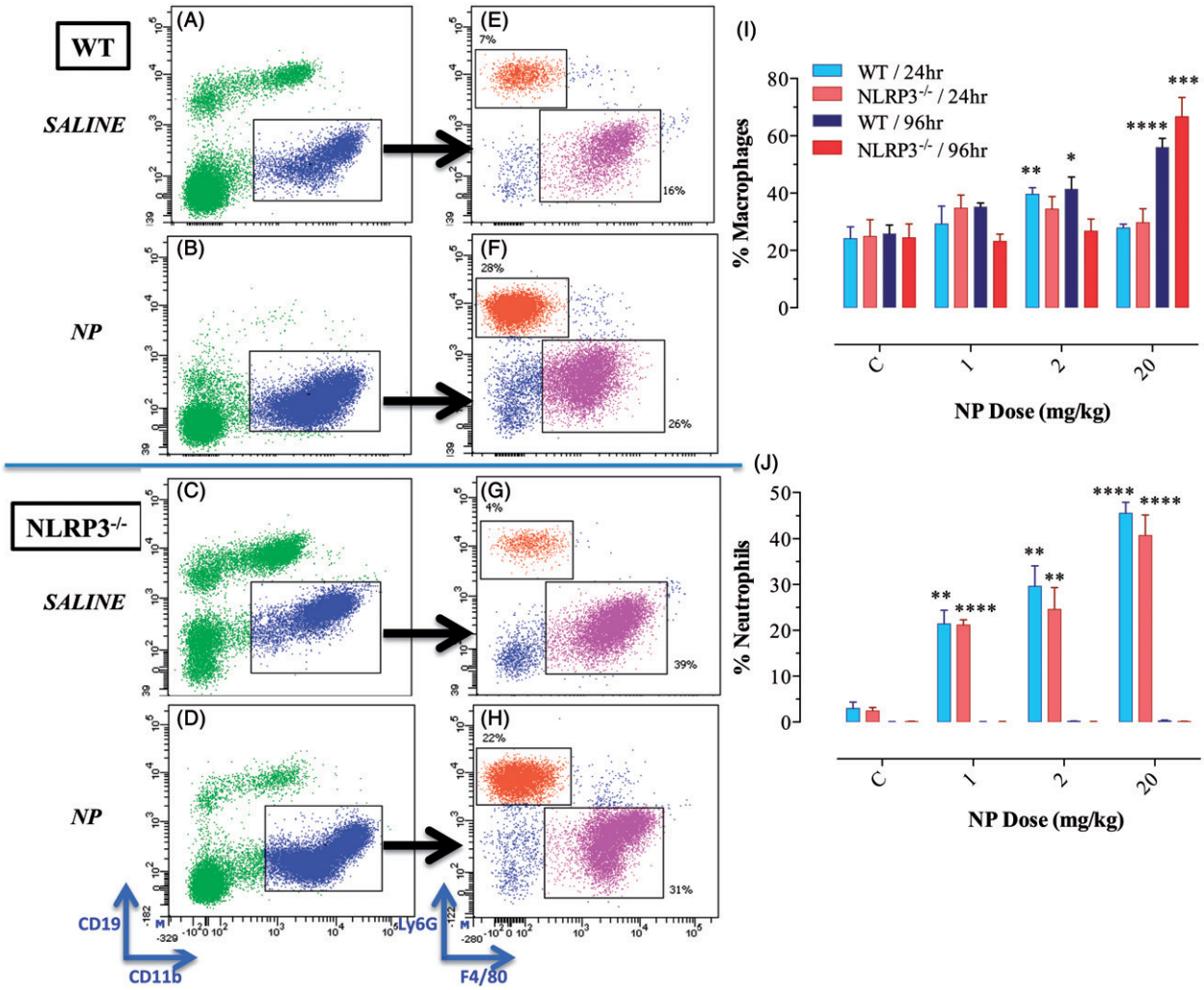

Figure 6. Flowcytometric analysis of PECs in mice exposed to NP. Cells were harvested from WT (panels A, B, E, F) or NLRP3$^{-/-}$ mice (C, D, G, H) 24 h or 96 h (*I*, *J*) after administration of either saline (A, C, E, G) or 2 mg/kg NP (B, D, F, H) and analyzed using a six-color panel of mAbs specific to CD11b, F4/80, Ly6G, CD19, and CD3. Non-viable cells were gated out by virtue of staining with 7AAD. Representative panels *A–D* show the pattern of staining with CD11b and CD19 mAbs. Gating on myeloid cells (CD11b^{+} CD19^{-}) allows the identification of macrophages (F4/80^{+}) and neutrophils (Ly6G^{+}), as shown in panels E–H. The bar graphs (panels I–J) depict the percent positive macrophages and neutrophils in control or NP-injected mice using three different doses, as indicated. Analysis was carried out in the different experimental groups at 24 h and 96 h time points and represents the means of 4–6 mice per group. The data is representative of three independent experiments. Asterisks denote significant differences between the indicated experimental group and its corresponding control group (*$p \leq 0.05$, **$p \leq 0.01$, ***$p \leq 0.001$, ****$p \leq 0.0001$).

increased neutrophil ratios in the bronchoalveolar lavage fluid (Arai et al., 2014; Smulders et al., 2014). Chronic dermal exposure to AgNP in guinea pigs resulted in deposition mainly in kidney, muscle and bone and was associated with toxicities (Korani et al., 2013). In these models, the effect of exposure to AgNP was studied over a long period of time (up to 35 days), reflecting chronic exposure consequences.

The effect of systemic exposure to AgNP has been investigated in a few studies (Li et al., 2014; Sarhan & Hussein, 2014). Intravenous administration of AgNP in mice, at doses ranging from 1 to 25 mg/kg, resulted over a period of 2–5 days in their deposition in the liver and induction of organ oxidative damage (Li et al., 2014). In another study, rats were given two intraperitoneal injections of a large dose of AgNP (2000 mg/kg) and analyzed 3 days later (Sarhan & Hussein, 2014). This treatment was found to induce elevated serum urea, creatinine, AST and ALT levels and organ toxicities documented by clear histological changes observed in kidney and liver (Sarhan & Hussein, 2014). However, the acute consequences of NP exposure have not been determined. Furthermore, the precise mechanisms involved in NP toxicity are not fully understood.

In our acute exposure model, systemic administration of Ag nanoalloys resulted in their rapid preferential deposition in the liver and led to hepatic toxicity. Previously, it was shown that systemic exposure to NP results in their accumulation within lysomal granules of liver Kupffer cells where they may reside for several months (Sadauskas et al., 2009, 2007). A recent *in vitro* study comparing the effect of different types of nanomaterials on a human hepatocyte cell line found that AgNP elicited the greatest level of cytotoxicity (Kermanizadeh et al., 2013). Our data demonstrate that systemic NP administration leads to elevated liver enzymes, which is consistent with the histological evidence of hepatic toxicity, including increase in sinusoidal Kupffer cells, foci of lobular granuloma and abscess formation. A dramatic increase in liver expression of inflammatory mediators (S100A9, IL-1β and IL-6), as well as histological alterations within the liver tissue, is clearly observed at 24 h post-exposure. However, the extent of these observed alterations was significantly attenuated in NLRP3$^{-/-}$ mice.

Phagocytic uptake of NP and their processing by lysosomes are two important steps that are required for the activation of NLRP3 inflammasome in macrophages (Wang et al., 2012).

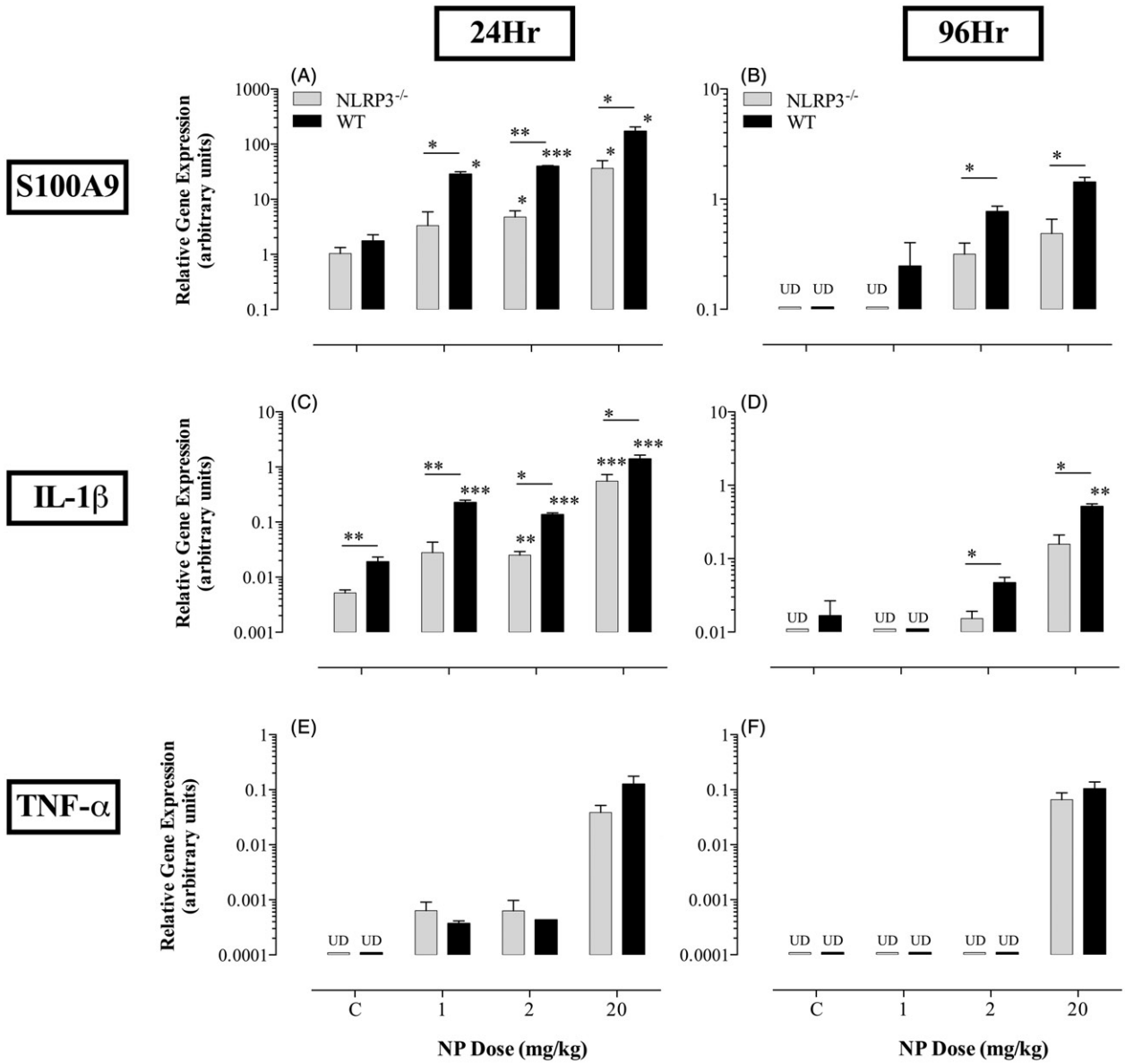

Figure 7. Induction of inflammatory mediators following NP exposure is partially dependent on the NLRP3 inflammasome. Relative gene expression levels of S100A9 (panels A–B), IL-1β (panels C–D) and TNF-α (panels E–F) in peritoneal cells of WT or NLRP3$^{-/-}$ mice. Cells were obtained from saline (control group) or NP-injected mice at 24 h or 96 h post-NP exposure. The NP doses used for inoculation were 1, 2, and 20 mg/kg bw, as indicated. Each data point represents the mean ± SEM of three mice per group. Asterisks denote statistically significant differences between the responses in WT and NLRP3$^{-/-}$ mice (*$p \leq 0.05$, **$p \leq 0.01$, ***$p \leq 0.001$). Additionally, when present, asterisks above each bar denote significant differences in comparison to the corresponding control group. The results are representative of three independent experiments.

The NLRP3 inflammasome regulates the activity of caspase-1, which in turn is responsible for the cleavage of pro-IL-1β to mature IL-1β protein (Sutterwala et al., 2006). S100A9 is an important recognition molecule of endogenous danger signals in phagocytes and regulates myeloid cell function by binding to TLR-4 (Ehrchen et al., 2009; Vogl et al., 2007). S100A9 dimerizes with S100A8 to form a complex (known as calprotectin), which is found predominantly in myeloid cells, and is actively secreted in response to stress in phagocytic cells (Markowitz & Carson, 2013). S100A9 belongs to a family of so-called damage associated molecular patterns (DAMPs) and were recently shown to have the capacity to regulate the activity of the NLRP3 inflammasome (Simard et al., 2013). The addition of S100A9 to human monocytes induced the secretion of several cytokines and chemokines, including IL-1β, IL-6, TNF-α and IL-8, through the activation of NF-κB in a process intimately linked to the generation of ROS (Simard et al., 2013). Furthermore, induction of IL-1β secretion was shown to occur via NF-κB-mediated activation of the NLRP3 inflammasome. Thus, it is feasible to conclude that exposure to NP induces cellular stress leading to the generation of S100A9 and ROS formation. This, in turn, leads to the activation of NF-κB which upregulates gene expression of many inflammatory cytokines and chemokines. Additionally, NF-κB increases the activity of NLRP3 which allows the maturation and synthesis of IL-1β cytokine. The finding that NP-induced S100A9 gene expression was also decreased in NLRP3$^{-/-}$ mice suggests the existence of a positive feedback loop involving NLRP3 and S100A9 protein in the response to nanoalloys.

An intriguing finding from our study is the apparent delay in the development of hepatic symptoms in NLRP3$^{-/-}$ mice following NP exposure. In contrast to WT mice whose hepatic responses begin to normalize by 96 h post-exposure, NLRP3$^{-/-}$ mice present with apparently a worsening or delayed response

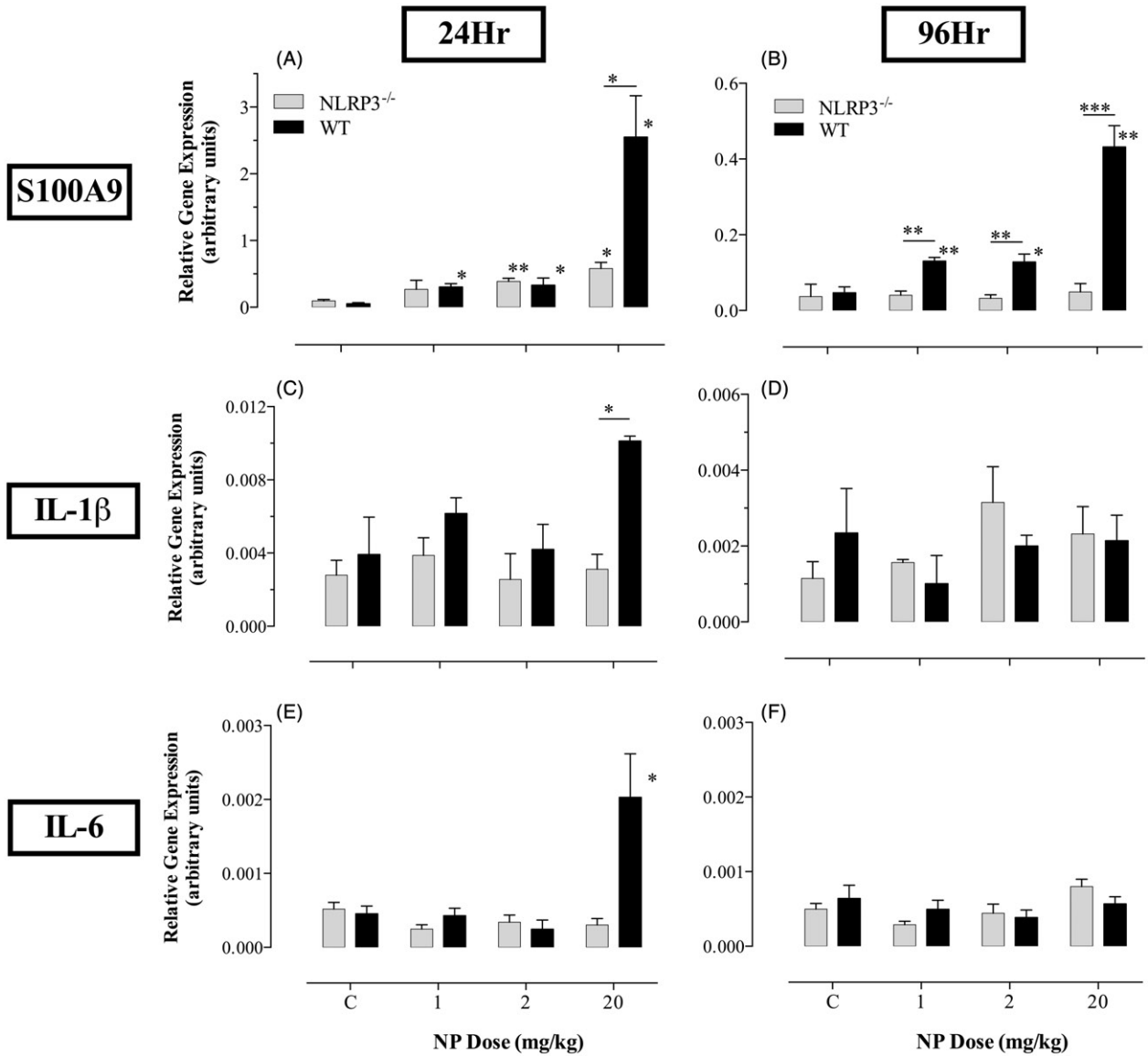

Figure 8. Increased expression of inflammatory genes in liver tissue following NP exposure. WT and NLRP3$^{-/-}$ mice were injected i.p. with NP (1, 2 or 20 mg/kg bw) and analyzed for expression of S100A9 (A–B), IL-1β (C–D) and IL-6 (E–F) genes at 24 h or 96 h later, as indicated. Each data point represents the mean ± SEM of three mice per group. Asterisks denote statistically significant differences between the responses in WT and NALP3$^{-/-}$ mice (*$p \leq 0.05$, **$p \leq 0.01$, ***$p \leq 0.001$). Additionally, when present, asterisks above each bar denote significant differences in comparison to the corresponding control group. The results are representative of two independent experiments.

profile. This can be clearly seen from the histological analysis of hepatic tissue and the persistent increase in ALT and LDH serum levels. The hepatic alterations observed at 96 h, including lobular granulomas, were associated with inflammatory infiltrates that were not seen at the earlier time point. This suggests that the late response to AgNP in NLRP3$^{-/-}$ mice may occur via a different pathway not involving this inflammasome. Moreover, the resolution of the hepatic manifestations in WT mice by 96 h reflects the liver's capacity for rapid regeneration following acute injury due to NP exposure. It is established that within a few days, 90% of the liver mass lost to a partial hepatectomy, for example, can be restored by hepatocyte proliferation of the remaining liver tissue (Yimlamai et al., 2014).

The hepatic alterations observed in our study extend previous findings that described changes in expression profile in murine livers following the administration of high dose AgNP via oral gavage (Cha et al., 2008). Microarray analysis of liver tissue revealed upregulated expression of the chemokine CXCL13 and the macrophage scavenger receptor, MARCO (Cha et al., 2008). CXCL13 mediates the recruitment of mononuclear cells and granulocytes into sites of inflammation (Mendez-Enriquez et al., 2008). The class A scavenger receptor MARCO (macrophage-associated receptor with collagenous structure) mediates opsonin-independent phagocytosis of particles, and hence contributes to their clearance (Getts et al., 2014; Palecanda & Kobzik, 2001). Moreover, exposure to NP inhibits the expression of the nuclear receptor Rev-erbβ, whose multiple functions include the negative regulation of macrophage activity and proinflammatory cytokine secretion as well as hepatocyte metabolism (Bugge et al., 2012; Cabrero et al., 2002). Together with our current findings on NP-induced hepatic alterations, these data demonstrate the profound effect of NP exposure on liver physiology and function. The involvement of the liver as a target of NP has also been observed in human patients (Trop et al., 2006). Treatment of a severe burn patient with silver-coated wound dressing caused elevated liver enzymes and subsequent symptoms of liver toxicity. Upon removing the wound dressing, the symptoms subsided, notwithstanding the patient's original condition. This suggested

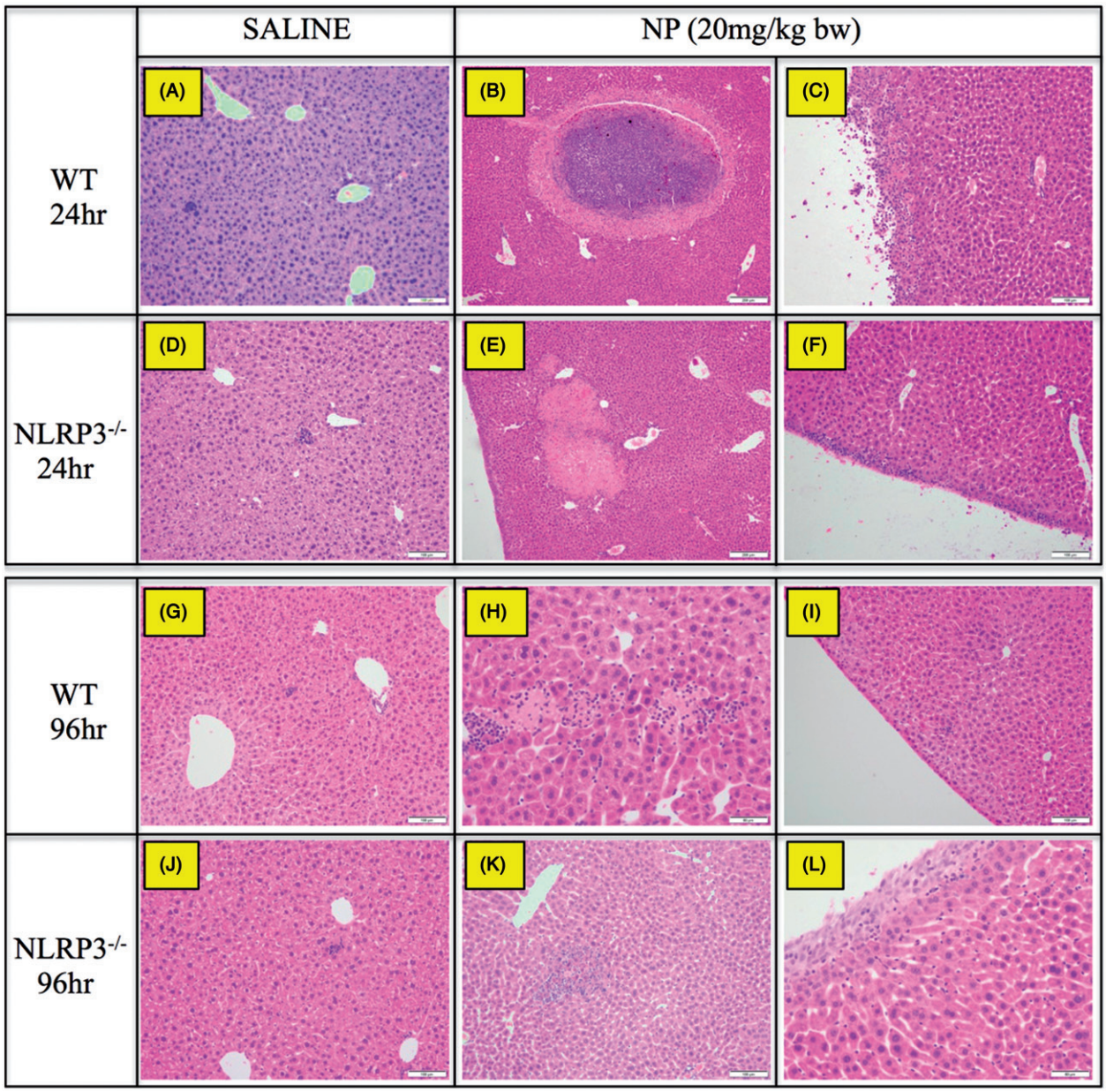

Figure 9. Histological analysis of liver tissue following NP exposure. WT and NLRP3$^{-/-}$mice (three mice per group) were exposed to different concentrations of NP (1, 2, 20 mg/kg body weight) and liver tissue sections were prepared 24 h (panels A–F) or 96 h (panels G–L) later. The images shown here are from animals exposed to the 20 mg/kg NP dose or saline-injected controls, as indicated. Panels B, E; scale bar = 200 μm; panels A, C–D, F–G, I, J–K; scale bar = 100 μm; panels H, L; scale bar = 50 μm. The results are representative of two independent experiments.

that Ag-coated dressing delivered a large dose of Ag to the body, which concentrated in the liver, causing toxicity symptoms (Trop et al., 2006).

Intraperitoneal injection of Ag-based nanoalloys led to a rapid infiltration of neutrophils into the peritoneal cavity. It is noteworthy that the extent of myeloid cell influx is similar in both WT and NLRP3-deficient mice. Previously, it was demonstrated that neutrophil recruitment in response to i.p. injection of TiO_2 NP was dependent primarily on IL-1α but not the NLRP3 inflammasome (Yazdi et al., 2010). In contrast to IL-1β, IL-1α is synthesized in an active form and does not require activation of the NLRP3 inflammasome for its production. Rather, it is rapidly secreted in response to cellular damage, thus acting as an alarmin that signals the host defense response (Lamacchia et al., 2013). Thus, the lack of any observed effect on cellular infiltration in NP-injected NLRP3$^{-/-}$ mice may be due to a similar mechanism. Moreover, administration of NP led to a dramatic increase in the expression of several proinflammatory genes in PECs including IL-1β, TNF-α and S100A9, a response that was significantly attenuated in NLRP3$^{-/-}$ mice. Nevertheless, it is important to note that despite decreased cytokine response in PECs of NLRP3$^{-/-}$ mice, significant induction of all three inflammatory cytokines (S100A9, IL-1β and TNF-α) was still evident. In fact, close inspection of the gene expression data in PECs suggests that the background expression of IL1β gene, and to a lesser extent S100A9 gene, appears to be at a lower level in NLRP3$^{-/-}$ mice compared to WT mice, resulting in equivalent fold-increases in gene expression in both mouse strains. Interestingly, this was observed in PEC but not in the liver, perhaps reflecting differential cytokine gene expression profiles in different cell populations with varying dependence on NLRP3. Thus, the equivalent induction of IL-1β gene expression that was observed in peritoneal macrophages of both WT and NLRP3$^{-/-}$ mice may well be the result of the induced expression of S100A9 protein following NP exposure. Our findings suggest that NP-induced, intraperitoneal recruitment of neutrophilic granulocytes and

increased gene expression of inflammatory mediators, particularly IL-1β, occur independently of NLRP3$^{-/-}$ inflammasome.

The range of doses used in our study (1–20 mg/kg) reflects cumulative levels that could be achieved in humans after repeated administration of NP. For example, for liposome-encapsulated doxorubicin NP used in cancer therapy, pharmokinetic data established plasma concentrations of more than 10 μg/ml (Gabizon et al., 1994). Similarly, concentrations of >10 mg/kg of liposomal NP have been reported in patients after repeated dosing and those were associated with prolonged thrombocytopenia (Golan et al., 2015). It is interesting to note that in our study, injection of NP at a dose of 2 mg/kg also resulted in significant reduction in circulating platelet numbers.

Taken together with previous findings, the current data highlight the need for caution to be taken to limit human exposure to different forms of NP and to devise means to reduce their toxicity. Elucidating the mechanism of NP-induced inflammation and the critical role played by the NLRP3 inflammasome suggests possible avenues to ameliorate the undesired consequences. For example, using novel bioengineering approaches, NP can be coated with NLRP-3 inhibitors (Coll et al., 2015; Youm et al., 2015), thereby potentially minimizing the resulting toxicity associated with NP administration and allowing their continued utilization as effective tools in diverse biomedical applications (Johnston et al., 2013).

Acknowledgements

The authors wish to thank Dr. Richard Flavell (Yale University School of Medicine, New Haven, CT) for his generous gift of the NLRP3$^{-/-}$ mice. We thank Arshad Khan for animal care and husbandry.

Declaration of interest

The authors declare no conflict of interest.

This work was funded by a grant from the United Arab University Research Office (to Y.H. and B.K.A) and in part by a grant from the Terry Fox Cancer Research Fund (to B.K.A.).

References

al-Ramadi BK, Fernandez-Cabezudo MJ, Ullah A, El-Hasasna H, Flavell RA. 2006. CD154 is essential for protective immunity in experimental salmonella infection: evidence for a dual role in innate and adaptive immune responses. J Immunol 176:496–506.

al-Ramadi BK, Fernandez-Cabezudo MJ, El-Hasasna H, Al-Salam S, Bashir G, Chouaib S. 2009. Potent anti-tumor activity of systemically-administered IL2-expressing Salmonella correlates with decreased angiogenesis and enhanced tumor apoptosis. Clin Immunol 130:89–97.

Arai Y, Miyayama T, Hirano S. 2014. Difference in the toxicity mechanism between ion and nanoparticle forms of silver in the mouse lung and in macrophages. Toxicology 328:84–92.

Bergin IL, Wilding LA, Morishita M, Walacavage K, Ault AP, Axson JL, et al. 2016. Effects of particle size and coating on toxicologic parameters, fecal elimination kinetics and tissue distribution of acutely ingested silver nanoparticles in a mouse model. Nanotoxicology 10: 352–60.

Borm PJ. 2002. Particle toxicology: from coal mining to nanotechnology. Inhal Toxicol 14:311–24.

Bugge A, Feng D, Everett LJ, Briggs ER, Mullican SE, Wang F, et al. 2012. Rev-erbα and Rev-erbβ coordinately protect the circadian clock and normal metabolic function. Genes Dev 26:657–67.

Cabrero A, Laguna JC, Vazquez M. 2002. Peroxisome proliferator-activated receptors and the control of inflammation. Curr Drug Targets Inflamm Allergy 1:243–8.

Carlson C, Hussain SM, Schrand AM, Braydich-Stolle LK, Hess KL, Jones RL, Schlager JJ. 2008. Unique cellular interaction of silver nanoparticles: size-dependent generation of reactive oxygen species. J Phys Chem B 112:13608–19.

Cha K, Hong HW, Choi YG, Lee MJ, Park JH, Chae HK, et al. 2008. Comparison of acute responses of mice livers to short-term exposure to nano-sized or micro-sized silver particles. Biotechnol Lett 30:1893–9.

Chen M, von Mikecz A. 2005. Formation of nucleoplasmic protein aggregates impairs nuclear function in response to SiO_2 nanoparticles. Exp Cell Res 305:51–62.

Coll RC, Robertson AA, Chae JJ, Higgins SC, Munoz-Planillo R, Inserra MC, et al. 2015. A small-molecule inhibitor of the NLRP3 inflammasome for the treatment of inflammatory diseases. Nat Med 21:248–55.

Dos Santos CA, Seckler MM, Ingle AP, Gupta I, Galdiero S, Galdiero M, et al. 2014. Silver nanoparticles: therapeutical uses, toxicity, and safety issues. J Pharm Sci 103:1931–44.

Ebabe Elle R, Gaillet S, Vide J, Romain C, Lauret C, Rugani N, et al. 2013. Dietary exposure to silver nanoparticles in Sprague-Dawley rats: effects on oxidative stress and inflammation. Food Chem Toxicol 60: 297–301.

Ehrchen JM, Sunderkotter C, Foell D, Vogl T, Roth J. 2009. The endogenous Toll-like receptor 4 agonist S100A8/S100A9 (calprotectin) as innate amplifier of infection, autoimmunity, and cancer. J Leukocyte Biol 86:557–66.

Fernandez-Cabezudo MJ, El-Kharrag R, Torab F, Bashir G, George JA, El-Taji H, al-Ramadi BK. 2013. Intravenous administration of manuka honey inhibits tumor growth and improves host survival when used in combination with chemotherapy in a melanoma mouse model. PLoS One 8:e55993.

Fernandez-Cabezudo MJ, Ali SA, Ullah A, Hasan MY, Kosanovic M, Fahim MA, et al. 2007. Pronounced susceptibility to infection by Salmonella enterica serovar Typhimurium in mice chronically exposed to lead correlates with a shift to Th2-type immune responses. Toxicol Appl Pharmacol 218:215–26.

Foldbjerg R, Olesen P, Hougaard M, Dang DA, Hoffmann HJ, Autrup H. 2009. PVP-coated silver nanoparticles and silver ions induce reactive oxygen species, apoptosis and necrosis in THP-1 monocytes. Toxicol Lett 190:156–62.

Gabizon A, Isacson R, Libson E, Kaufman B, Uziely B, Catane R, et al. 1994. Clinical studies of liposome-encapsulated doxorubicin. Acta Oncol 33:779–86.

Getts DR, Terry RL, Getts MT, Deffrasnes C, Muller M, van Vreden C, et al. 2014. Therapeutic inflammatory monocyte modulation using immune-modifying microparticles. Sci Transl Med 6:219–17.

Golan T, Grenader T, Ohana P, Amitay Y, Shmeeda H, La-Beck NM, et al. 2015. Pegylated liposomal mitomycin C prodrug enhances tolerance of mitomycin C: a phase 1 study in advanced solid tumor patients. Cancer Med 4:1472–83.

Issac JM, Sarawathiamma D, Al-Ketbi MI, Azimullah S, Al-Ojali SM, Mohamed YA, et al. 2013. Differential outcome of infection with attenuated Salmonella in MyD88-deficient mice is dependent on the route of administration. Immunobiology 218:52–63.

Johnston H, Pojana G, Zuin S, Jacobsen NR, Moller P, Loft S, et al. 2013. Engineered nanomaterial risk. Lessons learnt from completed nanotoxicology studies: potential solutions to current and future challenges. Crit Rev Toxicol 43:1–20.

Jung HJ, Pak PJ, Park SH, Ju JE, Kim JS, Lee HS, Chung N. 2014. Silver wire amplifies the signaling mechanism for IL-1beta production more than silver submicroparticles in human monocytic THP-1 cells. PLoS One 9:e112256.

Kaimala S, Mohamed YA, Nader N, Issac J, Elkord E, Chouaib S, et al. 2014. Salmonella-mediated tumor regression involves targeting of tumor myeloid suppressor cells causing a shift to M1-like phenotype and reduction in suppressive capacity. Cancer Immunol Immunother: CII 63:587–99.

Kermanizadeh A, Pojana G, Gaiser BK, Birkedal R, Bilanicova D, Wallin H, et al. 2013. In vitro assessment of engineered nanomaterials using a hepatocyte cell line: cytotoxicity, pro-inflammatory cytokines and functional markers. Nanotoxicology 7:301–13.

Kim JS, Kuk E, Yu KN, Kim JH, Park SJ, Lee HJ, et al. 2007. Antimicrobial effects of silver nanoparticles. Nanomedicine 3:95–101.

Kim YS, Song MY, Park JD, Song KS, Ryu HR, Chung YH, et al. 2010. Subchronic oral toxicity of silver nanoparticles. Particle Fibre Toxicol 7:20.

Korani M, Rezayat SM, Arbabi Bidgoli S. 2013. Sub-chronic dermal toxicity of silver nanoparticles in guinea pig: special emphasis to heart, bone and kidney toxicities. Iran J Pharm Res 12:511–19.

Lamacchia C, Rodriguez E, Palmer G, Gabay C. 2013. Endogenous IL-1α is a chromatin-associated protein in mouse macrophages. Cytokine 63: 135–44.

Li Y, Bhalli JA, Ding W, Yan J, Pearce MG, Sadiq R, et al. 2014. Cytotoxicity and genotoxicity assessment of silver nanoparticles in mouse. Nanotoxicology 8:36–45.

Markowitz J, Carson 3rd WE. 2013. Review of S100A9 biology and its role in cancer. Biochim Biophys Acta 1835:100–9.

Mendez-Enriquez E, Melendez Y, Martinez F, Baay G, Huerta-Yepez S, Gonzalez-Bonilla C, et al. 2008. CDIP-2, a synthetic peptide derived from chemokine (C-C motif) ligand 13 (CCL13), ameliorates allergic airway inflammation. Clin Exp Immunol 152:354–63.

Nel A, Xia T, Madler L, Li N. 2006. Toxic potential of materials at the nanolevel. Science 311:622–7.

Nemmar A, Albarwani S, Beegam S, Yuvaraju P, Yasin J, Attoub S, Ali BH. 2014. Amorphous silica nanoparticles impair vascular homeostasis and induce systemic inflammation. Int J Nanomed 9:2779–89.

Palecanda A, Kobzik L. 2001. Receptors for unopsonized particles: the role of alveolar macrophage scavenger receptors. Curr Mol Med 1:589–95.

Park EJ, Choi K, Park K. 2011. Induction of inflammatory responses and gene expression by intratracheal instillation of silver nanoparticles in mice. Arch Pharm Res 34:299–307.

Peeters PM, Perkins TN, Wouters EF, Mossman BT, Reynaert NL. 2013. Silica induces NLRP3 inflammasome activation in human lung epithelial cells. Particle Fibre Toxicol 10:3.

Reisetter AC, Stebounova LV, Baltrusaitis J, Powers L, Gupta A, Grassian VH, Monick MM. 2011. Induction of inflammasome-dependent pyroptosis by carbon black nanoparticles. J Biol Chem 286:21844–52.

Sadauskas E, Danscher G, Stoltenberg M, Vogel U, Larsen A, Wallin H. 2009. Protracted elimination of gold nanoparticles from mouse liver. Nanomedicine 5:162–9.

Sadauskas E, Wallin H, Stoltenberg M, Vogel U, Doering P, Larsen A, Danscher G. 2007. Kupffer cells are central in the removal of nanoparticles from the organism. Particle Fibre Toxicol 4:10.

Sarhan OM, Hussein RM. 2014. Effects of intraperitoneally injected silver nanoparticles on histological structures and blood parameters in the albino rat. Int J Nanomed 9:1505–17.

Simard JC, Vallieres F, de Liz R, Lavastre V, Girard D. 2015. Silver nanoparticles induce degradation of the endoplasmic reticulum stress sensor activating transcription factor-6 leading to activation of the NLRP-3 inflammasome. J Biol Chem 290:5926–39.

Simard JC, Cesaro A, Chapeton-Montes J, Tardif M, Antoine F, Girard D, Tessier PA. 2013. S100A8 and S100A9 induce cytokine expression and regulate the NLRP3 inflammasome via ROS-dependent activation of NF-κB(1.). PLoS One 8:e72138.

Smulders S, Luyts K, Brabants G, Landuyt KV, Kirschhock C, Smolders E, et al. 2014. Toxicity of nanoparticles embedded in paints compared with pristine nanoparticles in mice. Toxicol Sci 141: 132–40.

Sun B, Wang X, Ji Z, Li R, Xia T. 2013. NLRP3 inflammasome activation induced by engineered nanomaterials. Small 9:1595–607.

Sung JH, Ji JH, Park JD, Yoon JU, Kim DS, Jeon KS, et al. 2009. Subchronic inhalation toxicity of silver nanoparticles. Toxicol Sci 108: 452–61.

Sutterwala FS, Ogura Y, Szczepanik M, Lara-Tejero M, Lichtenberger GS, Grant EP, et al. 2006. Critical role for NALP3/CIAS1/Cryopyrin in innate and adaptive immunity through its regulation of caspase-1. Immunity 24:317–27.

Trop M, Novak M, Rodl S, Hellbom B, Kroell W, Goessler W. 2006. Silver-coated dressing acticoat caused raised liver enzymes and argyria-like symptoms in burn patient. J Trauma 60:648–52.

Valsami-Jones E, Lynch I. 2015. NANOSAFETY. How safe are nanomaterials? Science 350:388–9.

Vogl T, Tenbrock K, Ludwig S, Leukert N, Ehrhardt C, van Zoelen MA, et al. 2007. Mrp8 and Mrp14 are endogenous activators of Toll-like receptor 4, promoting lethal, endotoxin-induced shock. Nat Med 13: 1042–9.

Wang X, Xia T, Duch MC, Ji Z, Zhang H, Li R, et al. 2012. Pluronic F108 coating decreases the lung fibrosis potential of multiwall carbon nanotubes by reducing lysosomal injury. Nano Lett 12:3050–61.

Winter M, Beer HD, Hornung V, Kramer U, Schins RP, Forster I. 2011. Activation of the inflammasome by amorphous silica and TiO_2 nanoparticles in murine dendritic cells. Nanotoxicology 5:326–40.

Yang EJ, Kim S, Kim JS, Choi IH. 2012. Inflammasome formation and IL-1β release by human blood monocytes in response to silver nanoparticles. Biomaterials 33:6858–67.

Yazdi AS, Guarda G, Riteau N, Drexler SK, Tardivel A, Couillin I, Tschopp J. 2010. Nanoparticles activate the NLR pyrin domain containing 3 (Nlrp3) inflammasome and cause pulmonary inflammation through release of IL-1alpha and IL-1beta. Proc Natl Acad Sci USA 107:19449–54.

Yimlamai D, Christodoulou C, Galli GG, Yanger K, Pepe-Mooney B, Gurung B, et al. 2014. Hippo pathway activity influences liver cell fate. Cell 157:1324–38.

Youm YH, Nguyen KY, Grant RW, Goldberg EL, Bodogai M, Kim D, et al. 2015. The ketone metabolite β-hydroxybutyrate blocks NLRP3 inflammasome-mediated inflammatory disease. Nat Med 21: 263–9.

Supplementary material available online